applied optics

Analysis and experiment of a pneumatic-hydraulic composite support system for *in-situ* mirror processing and testing

Deyi Dong,[1] Di Zhou,[1,*] Haifei Hu,[1] Lianqiang Wang,[1] Chao Li,[1] Yuhan Jiang,[2] and Yingjun Guan[3]

[1]Changchun Institute of Optics, Fine Mechanics and Physics, Chinese Academy of Sciences, Changchun 130033, China
[2]Canon Medical System Research Development (Dalian) Co., Ltd., Dalian 116085, China
[3]College of Mechanical & Electrical Engineering, Changchun University of Technology, Changchun 130012, China
*zhoudi@ciomp.ac.cn

Received 7 August 2023; revised 17 September 2023; accepted 27 September 2023; posted 28 September 2023; published 16 October 2023

To address the deformation issues caused by the self-gravity and machining stresses in the process of large-aperture mirror fabrication, this paper proposes an *in-situ* switchable pneumatic-hydraulic hybrid supporting system that enables the seamless transition between machining and testing. By facilitating *in-situ* switching, this system not only reduces the machining time of large-aperture mirrors, thereby enhancing production efficiency, but also mitigates the risks associated with traditional switching methods that may result in mirror damage due to human error. Three typical working conditions of the hybrid supporting system, namely hydraulic machining support, air-floating testing support, and three-point rigid support, are investigated in terms of mirror loading through a finite element simulation. Additionally, an experimental platform is constructed to validate the proposed system. The experimental results affirm the feasibility of the designed pneumatic-hydraulic hybrid supporting system. This system will serve as a technological support to advance the rapid development of large-aperture space telescope manufacturing techniques.

https://doi.org/10.1364/AO.502722

1. INTRODUCTION

Space telescopes are crucial instruments for human exploration of the universe. The larger the aperture of a telescope, the higher is its resolution, allowing for stronger observations of unexplored regions in the universe. Notable examples include the 2.4-m Hubble Space Telescope (HST) [1], launched by the United States in 1990 and still in service, the Airborne Observatory SOFIA [2], which began operations in 2010, the 6.5-m James Webb Space Telescope (JWST) [3] launched in 2021, and the Herschel Space Observatory launched by Europe in 2009 [4]. In order to obtain clear imaging, the primary mirror of a telescope not only requires extremely high surface accuracy and low surface roughness, but also imposes stringent requirements for mirror manufacturing and testing under the microgravity environment. Traditional methods for the measuring surface shape in a microgravity environment involve multi-orientation shape measurement techniques. These methods detect the mirror's shape changes in different orientations and use interpolation or averaging algorithms to predict the mirror's shape in a zero-gravity condition. Examples of such methods include the suspended flipping testing scheme developed by Jet Propulsion Laboratory (JPL) [5] and the offline flipping testing scheme used by Tinsley for the James Webb Space Telescope (JWST) [6,7]. However, these flipping testing methods carry certain risks, especially when dealing with large-aperture mirrors, as the flipping process can easily lead to damage. To mitigate this risk, *in-situ* testing methods have been developed at the processing station, such as lever balance structures or hydraulic/pneumatic support techniques [8–10]. These methods use multi-point support to counterbalance the gravity on the mirror surface and simulate the measurement of the surface shape in a microgravity environment. In addition to the gravity unloading issue, stress relief during mirror polishing is also crucial. This is because the polishing tool exerts significant pressure on the mirror surface, causing elastic deformation (namely print-through effect) in the polishing area. After polishing, the original area undergoes elastic recovery, resulting in local errors. Therefore, this paper proposes a pneumatic-hydraulic composite support system, referred to as the PHCS (pneumatic–hydraulic composite support) system, which aims to simultaneously address the deformation caused by the mirror's own weight and the processing stress during mirror manufacturing.

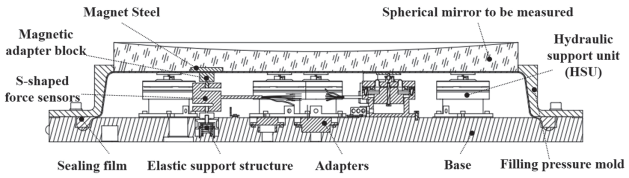

Fig. 1. Schematic of the pneumatic–hydraulic composite support (PHCS) system.

2. ILLUSTRATION OF PNEUMATIC–HYDRAULIC COMPOSITE SUPPORT SYSTEM

As depicted in Fig. 1, the PHCS system composes a processing support system and a testing support system. Its main objective is to facilitate the *in-situ* processing and testing of the mirror surface shape. During the polishing and shaping of the mirror, the hydraulic support system offers multi-point support force for the mirror body. Conversely, when the processed mirror is being inspected, the PHCS system seamlessly transitions to the air flotation support system. These two systems are seamlessly integrated, operate autonomously, and allow for swift switching between them.

The processing support system consists of nine hydraulic support units, each unit being a single-cylinder structure. The output force of these hydraulic support units exhibits a strictly linear relationship with the pipeline pressure. Additionally, within the same hydraulic circuit, the parallel hydraulic support units can be assumed to operate at the same working pressure, thus showcasing excellent force equality characteristics. This design effectively reduces the need for numerous sensors and controllers, resulting in significant cost savings compared to the double-cylinder support units used in MMT [11]. Moreover, the top design of these hydraulic support units features a ball–joint structure, which imparts axial stiffness, facilitating decoupling of stiffness in multiple axes and allowing for independent control of degrees of freedom. The stiffness characteristics and testing of these hydraulic support units have been described in detail in reference [12]; hence, we refrain from further elaboration in this paper. The diameter of the tested mirror is 500 mm, and the aspect ratio of the reflective mirror is 20:1. The arrangement of the nine processing support units composes three units uniformly distributed in the inner circle and six units uniformly distributed in the outer circle. The diameter of the inner circle's pitch circle is 180 mm, while the outer circle's pitch circle diameter is 420 mm. The placement of the support units is optimized based on a hierarchical iterative algorithm under the condition of equal force support, as provided in reference [13]. Therefore, it is assumed that the mirror's imprinting effect is minimized under this processing state.

The testing support system consists of a base, sealing film, film pressure mold, magnetic steel, three evenly distributed S-shaped force sensors, and an elastic support structure. The magnetic steel is bonded to three processing holes on the back of the tested mirror. The magnetic transfer component, S-shaped force sensors, and elastic support structure are connected in series, forming three axial positioning points, together with the magnetic steel. The film pressure mold serves two purposes: first, it exerts pressure on the spherical skirt edge of the sealing film to achieve sealing; secondly, it ensures that the force applied by the sealing film to the edge of the mirror body is normal to the contact surface.

The specific operation process of the PHCS system is follows: during the mirror processing, the hydraulic support units are filled with working fluid, raising the mirror to provide support from the back and unload the processing stress generated by the grinding tool. After each round of mirror shaping, the hydraulic support units are lowered to the lowest position, and the value displayed by the S-shaped force sensors is approximately one-third of the gravity acting on the mirror. At this point, the enclosed space composed of the base, sealing film, and film pressure mold is inflated until the value displayed by the S-shaped force sensors decreases to less than 1% of the original value. The *in-situ* testing optical path is then opened to obtain the surface form accuracy of the mirror in a gravity-free state.

The design of the PHCS system must adhere strictly to two key aspects. First, the system's sealing must be of high quality to ensure the stability of support stiffness during long-term operation, whether it is for processing or testing. Secondly, the system's axial stiffness needs to be maximized to guarantee precise support force during mirror processing. To ensure tightness, two design approaches are employed. First, the number of perforations in the system base is minimized to reduce the risk of leakage. Secondly, elastic materials are used as structural components between metal parts, allowing for sealing through elastic deformation. To achieve high support force accuracy, the working pressure should be maximized within a safe range, while minimizing the gas content in the working liquid.

3. SIMULATION ANALYSIS OF MIRROR SHAPES UNDER DIFFERENT WORKING CONDITIONS

In practical applications, the PHCS system exhibits three different support states in the axial direction. These states are as follows: the machining state, which corresponds to the nine-point hydraulic support (providing support and overcoming grinding tool pressure); the testing state, air flotation support (unloading mirror gravity); and the transition state, three-point support. (When the airbags are deflated and the hydraulic support units are not yet active, three force sensors and pads form an axial rigid support). A finite element simulation was conducted to evaluate the surface form accuracy of the mirror in each support state. The simulation was initialized with the conditions shown in Table 1, where three grooves were evenly distributed on a pitch circle with a diameter of 270 mm on the back of the mirror for placing magnetic steel. In the three-point support state, a support force equal to one-third of the gravity value was applied to each groove, and a virtual constraint was added at the center of the mirror's back surface to constrain six degrees of freedom. In the nine-point support state, hard points were set in advance using PATRAN software before meshing, corresponding to the positions of each hydraulic support unit, and support forces were applied at these positions, with a value equal to one-ninth of the mirror's gravity. Since both the pressure and position of the grinding tool affect the mirror's surface form, this state only simulated the initial state before processing, with a virtual constraint added at the center of the mirror's back surface to constrain six degrees of freedom. In the airbag support state, a pressure equal to the mirror's gravity was applied to the back

Table 1. Initial Conditions of FEM Simulation

Mirror's aperture	500 mm
Radius of curvature of the reflective surface	3000 mm
Center height of the mirror	25 mm
Material of the mirror	Crystallite
Grid element type of FEM	Hexahedron
Gravity direction	From the negative direction of Z-axis

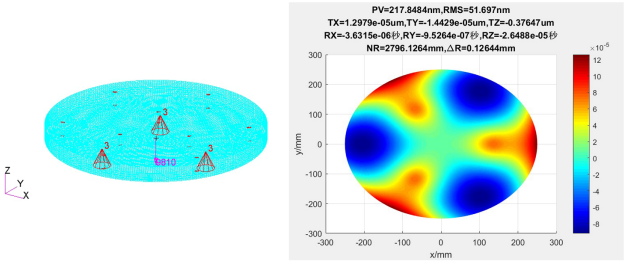

(a) (b)

Fig. 2. (a) Mirror simulation conditions under three-point support conditions. (b) Surface figure of the measured mirror and its deformation.

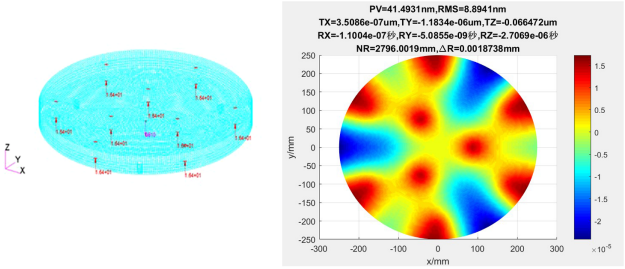

(a) (b)

Fig. 3. (a) Mirror simulation conditions under nine-point support conditions. (b) Surface figure of the measured mirror and its deformation.

surface, and fixed constraints were added to the three grooves on the back surface. The conditions and deformation contour maps for each support state are shown in Figs. 2–4. In the three-point support state, the mirror's PV value is approximately 0.344λ, with an RMS value of 0.082λ. In the nine-point support state, the mirror's PV value is approximately 0.066λ, with an RMS value of 0.014λ. In the airbag support state, the mirror's PV value is approximately 0.022λ, with an RMS value of 0.005λ.

By comparing the surface deformation contour maps of the three-point and nine-point support states, several similarities and differences can be observed. In both states, the mirror's center point remains undeformed due to the addition of a virtual constraint at the center of the mirror's back surface. The support points, on the other hand, correspond to the high points of the entire surface form, while positions farther from the center and support points correspond to the low points of the surface form. The main difference between the two states lies in the number of support points. As the nine-point support state has more support points, the surface deformation is more evenly distributed compared to the three-point state. Consequently, the

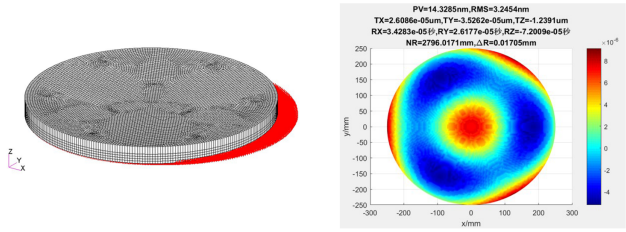

(a) (b)

Fig. 4. (a) Mirror simulation conditions under aerostatic support conditions. (b) Surface figure of the measured mirror and its deformation.

magnitudes of high and low points in the entire mirror surface are reduced by an order of magnitude in the nine-point support state. This leads to smaller PV and RMS values for the mirror's surface form in this state. From this perspective, it can be concluded that the nine-point support state is more suitable as a machining support state, especially when combined with the technology of combined grinding heads [14–16], as it efficiently unloads the processing stress and minimizes the imprinting effect on the mirror's surface form during the processing state.

As shown in Fig. 4, the three points fixed on the back of the mirror are consistent with the boundary conditions of the actual usage of this system. The axial positioning points composed of the three force sensors and pads maintain contact with the magnetic steel bonded to the back of the mirror throughout the transition process.

In the airbag support state, the deformation at the three fixed constraint points on the mirror is zero. This is due to the application of reverse pressure to counteract the gravity of the mirror. The nodes on the reflective surface that are far from the fixed constraint points, such as the center point and the edge of the mirror, become high points. Compared to the nine-point support state, the airbag support state provides the highest surface form accuracy for the mirror. This is because the airbag support state simulates the effect of numerous support points simultaneously applying support forces, and the pressure is uniformly distributed. Therefore, this support state is mainly used to simulate the change in the mirror's surface form accuracy after the release of gravity when a satellite carrying optical loads is launched into orbit.

4. EXPERIMENTAL PLATFORM SETUP

Based on the actual optical path requirements for testing, an *in-situ* optical platform for the PHCS system was constructed, as illustrated in Fig. 5. The principle of *in-situ* testing is that parallel light is emitted from a 4D interferometer (Phase Cam 6010) and, after passing through a beam expander and a flat mirror, it is directed onto the reflective surface of the test spherical mirror. One group of experimenters continuously adjusts the position of the test spherical mirror by rotating the three feet at the bottom of the composite support system. Another group of experimenters adjusts the 5D-adjustable frame of the 4D interferometer to ensure that the light reflected from the test spherical mirror enters the interferometer and reaches a detectable state.

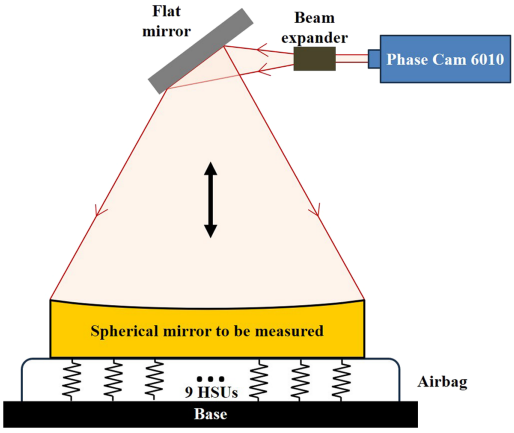

Fig. 5. Schematic of the experimental principle of the pneumatic–hydraulic composite support system.

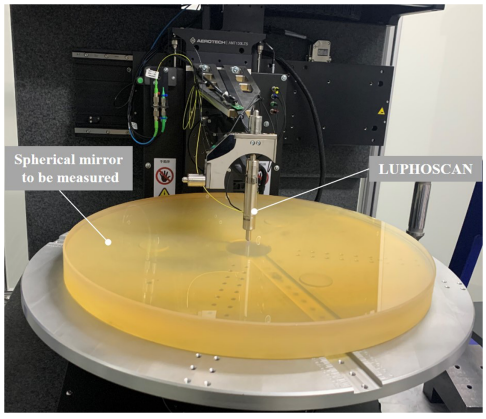

Fig. 6. Testing of the face shape accuracy of the single mirror with the LUPHOSCAN system.

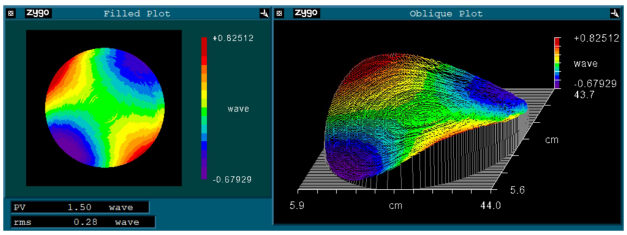

Fig. 7. Results of the single mirror's face shape before the removal of image distortion, spherical aberration, and coma.

As shown in Fig. 6, the surface form accuracy of the bare mirror was first measured using the LUPHOSCAN system. The PV value was determined to be 1.5λ, while the RMS value was measured to be 0.28λ, as shown in Fig. 7.

Subsequently, the assembly of the composite support system was carried out. In this process, the hydraulic units in the machining support were connected, along with the connector, ball valve, piezometer, peristaltic pump, and liquid bottle, to form a hydraulic circuit. The piezometer was connected to a laptop computer via a USB to TTL converter for pressure readings of the hydraulic circuit, as shown in Fig. 8(a). The connection of the hydraulic support units is illustrated by the yellow lines in Fig. 8(b), with the wiring of each S-type force

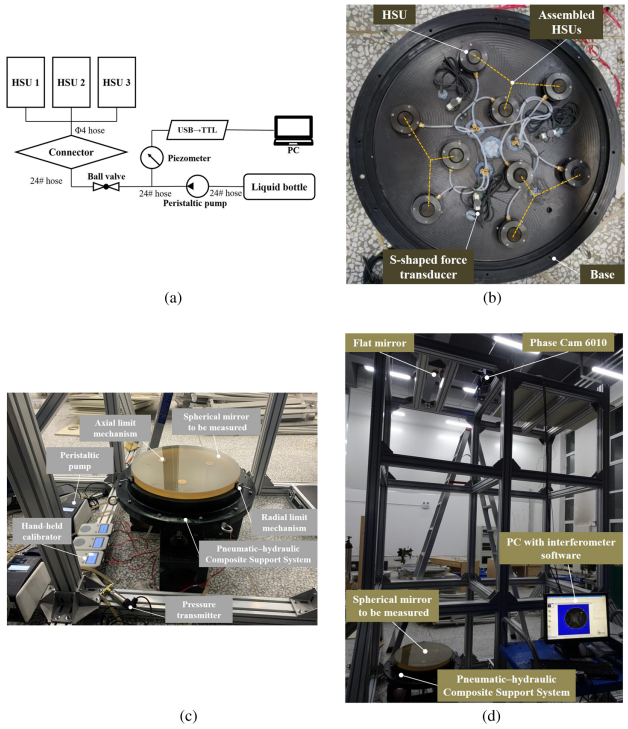

Fig. 8. (a) Schematic of the hydraulic circuit with respect to assembled HSUs. (b) Photo of the assembled hydraulic support system. (c) Assembled composite support system with hydraulic circuits. (d) Physical diagram of the optical test platform of the PHCS system.

sensor being adapted through aviation plugs and read using a handheld calibrator. The connections at the aviation plug interface and oil hole conversion interface were sealed with glass glue. In the PHCS system, shown in Fig. 8(c), both axial and radial limits were imposed on the spherical mirror. Axial limitation was achieved by the attraction between three magnetic steel pieces bonded to the mirror's back surface and the pads above the force sensors. Radial limitation was achieved through the design of three evenly distributed top rod structures. The built optical testing platform in Fig. 8(d) consisted of the PHCS system and accompanying measurement equipment, a 3 m high aluminum frame, a 100 mm diameter flat mirror and its fixture, a 4D interferometer, a five-dimensional adjustable frame, and a computer with interferometer measurement software.

5. RESULTS AND DISCUSSION

The reflective mirror surfaces in four different support states were tested using the built optical platform. Due to suboptimal edge processing of mirrors larger than 440 mm, which is unfavorable for data comparison, the aperture of the mirrors in all the test results was standardized to 440 mm after removing image distortion, spherical aberration, and coma, as shown in Figs. 9–12.

(a) In the bare mirror testing state, the reflective mirror surface was measured using the LUPHOSCAN system, with a PV value of 0.41λ and RMS of 0.06λ.
(b) In the three-point support state with an empty cavity, the reflective mirror surface was measured using a 4D

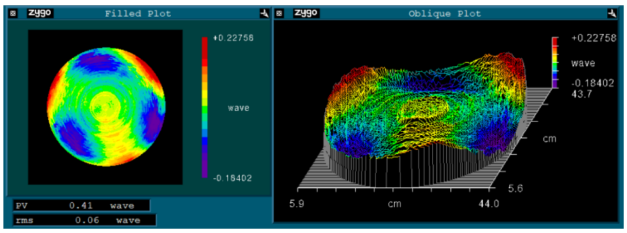

Fig. 9. Results of the single mirror's face shape.

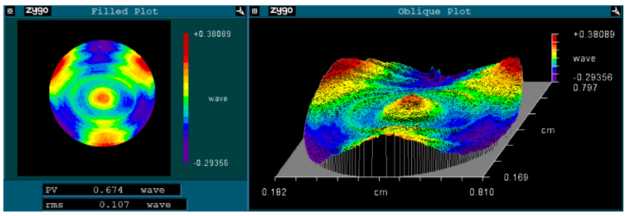

Fig. 10. Actual measurement results of the surface figure under three-point support conditions.

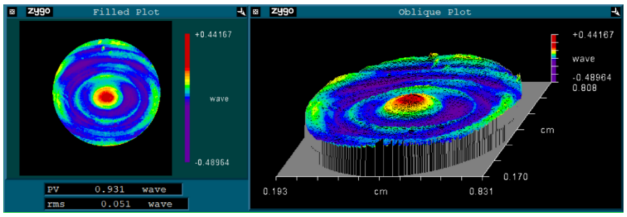

Fig. 11. Actual measurement results of the surface figure under nine-point support conditions.

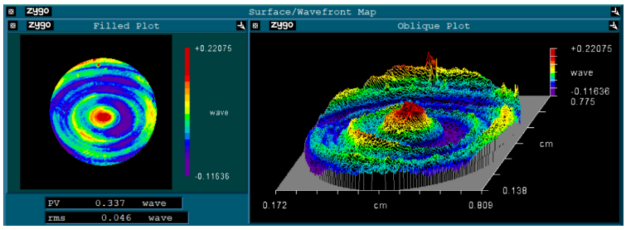

Fig. 12. Actual measurement results of the surface figure under aerostatic support conditions.

interferometer, with a PV value of 0.674λ and RMS of 0.107λ.

(c) In the nine-point support state with water-filled support units, simulating the support state during processing, the reflective mirror surface was measured using a 4D interferometer, with a PV value of 0.931λ and RMS of 0.051λ.

(d) In the airbag support state with an inflated cavity, simulating the support state during unloading gravity in testing, the reflective mirror surface was measured using a 4D interferometer, with a PV value of 0.337λ and RMS of 0.046λ.

However, there are areas for improvement in the experiment:

(a) Considering the development cost, the bare mirror surface underwent only rough processing, resulting in poor surface quality. This led to little difference between the quantitative surface deformation under the three operating conditions and the analysis results.

(b) Due to process-related issues, the thickness of the airbag membrane reached 1.2 mm, resulting in higher membrane stiffness. Therefore, the measured mirror surface deformations under the three states are influenced to some extent by the stiffness of the membrane material itself, which was not considered in the simulation.

(c) The effect of reversing the air using the peristaltic pump is not ideal, leading to non-uniform stiffness of each hydraulic support unit and dispersion of stiffness. Compared to the nine-point mechanical hard support that achieved equal height after grinding, the obtained actual surface deformation is slightly worse. An improvement approach could be to install exhaust devices (plug and solution buffer bottle) in the hydraulic support units and add ball valves between the peristaltic pump and support units in each branch to maintain stable pressure.

6. CONCLUSION

The proposed PHCS system in this study addresses the risks associated with multiple flips and transportation of large-aperture mirrors during the machining and inspection processes while avoiding positioning errors caused by multiple clamping. The composition and usage of the hybrid supporting system are elaborately introduced, followed by the machining and assembly of the system. A complementary optical inspection platform is also set up for *in-situ* testing. Based on an analysis through a simulation and experimental verification of the three typical working conditions, the functionality of the system is validated. Additionally, an error analysis is conducted on both the simulation and experimental results. This system will greatly improve the efficiency of large-aperture mirror fabrication and further advance the development of space telescope technology.

Funding. National Natural Science Foundation of China (11873007, 62175234).

Disclosures. The authors declare no conflicts of interest.

Data availability. Data underlying the results presented in this paper are not publicly available at this time but may be obtained from the authors upon reasonable request.

REFERENCES

1. L. D. Feinberg and P. H. Geithner, "Applying HST lessons learned to JWST," Proc. SPIE **7010**, 70100N (2008).
2. E. F. Erickson, "SOFIA: the next generation Airborne observatory," Space Sci. Rev. **74**, 91–100 (1995).
3. JWST, "The James Webb Space telescope," Space Sci. Rev. **123**, 485–606 (2006).
4. G. L. Pilbratt, J. R. Riedinger, T. Passvogel, G. Crone, and M. Schmidt, "Herschel space observatory–an ESA facility for far-infrared and submillimetre astronomy," Astron. Astrophys. **518**, L1-416 (2010).
5. E. E. Bloemhof, J. C. Lam, V. A. Feria, and Z. Chang, "Extracting the zero-gravity surface figure of a mirror through multiple clockings in a flightlike hexapod mount," Appl. Opt. **48**, 4239–4245 (2009).

6. D. L. Aronstein, "Optical Testing of the James Webb Space Telescope [EB/OL]," http://ntrs.nasa.gov/archive/nasa/casi.ntrs.nasa.gov/20140009178.pdf.
7. G. C. Cole, R. Garfield, T. Peters, W. Wolff, K. Johnson, R. Bernier, C. Kiikka, T. Nassar, H. A. Wong, and J. Kincade, "An overview of optical fabrication of the JWST mirror segments at Tinsley," Proc. SPIE **6265**, 62650V (2006).
8. P. R. Yoder, *Opto-Mechanical Systems Design*, 3rd ed. (SPIE, 2006).
9. H. F. Hu and X. Luo, "Design scheme for optical manufacturing support system of TMT M3 prototype," Proc. SPIE **9280**, 928006 (2014).
10. H. F. Hu, X. Luo, Z. Y. Liu, X. J. Zhang, and H. W. Zhao, "Designing a hydraulic support system for large monolithic mirror's precise in-situ testing-polishing iteration," Opt. Express **27**, 3746–3760 (2019).
11. H. M. Martin, R. G. Allen, B. Cuerden, S. T. Derigne, and S. Warner, "Primary mirror system for the first Magellan telescope," Proc. SPIE **4003**, 2–13 (2000).
12. D. Y. Dong, D. Zhou, Y. H. Jiang, L. Q. Wang, C. Li, H. F. Hu, Y. J. Guan, and M. H. Gao, "Stiffness analysis and verification of hydraulic supporting units for in-situ optical testing of a 500 mm-diameter mirror," Machines **10**, 828 (2022).
13. X. H. Xi, C. J. Zhang, H. F. Hu, and Y. J. Guan, "Layout-stiffness-correction force joint optimization of support system for ultra-large thin meniscus mirror," Opto-Electron Eng. **47**, 190551 (2020).
14. Z. Y. Liu, L. L. Xiang, X. F. Zeng, X. Luo, and X. J. Zhang, "Fabrication of large aspheric mirror using multi-mode polishing based on error separation," Opt. Precis. Eng. **25**, 813–819 (2017).
15. Y. S. Yao, M. A. Zhen, X. U. Liang, J. T. Ding, Y. J. Wang, L. Shen, and B. Jiang, "Removal functions of different polishing heads worked in planet motion model," Opt. Precis. Eng. **25**, 2706–2713 (2017).
16. W. Tang, W. J. Deng, X. L. Yin, D. L. Xue, L. G. Zheng, and X. J. Zhang, "Computation of the removal function for ion beam figuring curved surface," J. Comput. Theor. Nanosci. **13**, 7025–7031 (2016).